Research paper

Multifunctional polymeric composites for non-invasive visualization of deposits derived from experimental turbidity currents

Maria Helena da Silva Reis[a], Raiane Valenti Gonçalves[a], Natan Dias Martin[b], Fernando Lagni Martins[b], Mara Lise Zanini[b], Cássio Stein Moura[a,b,c], Ricardo Meurer Papaléo[a,b], Nara Regina de Souza Basso[a,b,*]

[a] Programa de Pós-Graduação em Engenharia e Tecnologia de Materiais, Pontifícia Universidade Católica do Rio Grande do Sul – PUCRS, Av. Ipiranga, 6681, Porto Alegre, RS, CEP 90619-900, Brazil
[b] Escola de Ciências, PUCRS, Brazil
[c] Institute of Petroleum and Natural Resources, PUCRS, Brazil

ABSTRACT

In this work, we report a new approach to non-invasive imaging of the internal architecture of sedimentary deposits from turbidity currents in hydraulic tank simulations. A composite material based on polyester resin, barium sulphate particles and different dyes newly developed enhances and controls optical and x-ray contrast of the deposited sediments. The composites presented specific mass and settling velocity, which varied slightly with composition, but were similar to those of coal, a material that is commonly used for small-scale sedimentation simulations. The addition of 2% (w/w) of barium sulphate provides the opacity required for detection by x-ray microtomography and the presence of dyes of vivid colors gives a natural contrast for optical imaging. The developed nanocomposites present suitable hydraulic properties combined with tunable multimodal contrast properties for non-invasive visualization, making them useful materials in physical simulations of sedimentary deposits from experimental turbidity currents.

1. Introduction

Turbidity currents are particle-laden gravity-driven underflows in which the particles are largely suspended by fluid turbulence. Typically, this turbulence is generated by the forward motion of the current along the lower boundary of the domain, the motion being in turn driven by the action of gravity on the density difference between the particle-fluid mixture and the ambient fluid (Meiburg and Kneller, 2010). Such currents are classified as conservative or non-conservative. The non-conservative density currents involve a greater number of variables and for such reason their behavior is more complex than conservative currents. This fact is due to the density variation in the non-conservative currents that occurs by the entrance and departure of particles in the middle of the current, whilst in the conservative currents the density variation happens only by the entrance of ambient fluid (Kneller and Buckee, 2000). Turbidity currents are a specific type of non-conservative density current in which the excess density is caused by the presence of sediment suspended in the turbulence of the surrounding fluid (Hasen et al., 2015; Chamoun et al., 2016).

Turbidity currents present a characteristic longitudinal profile composed of a head, body and tail (Allen, 1971; Simpson and Britter, 1979). The head of the turbidity current located on its front region has a geometric characteristic of a semi ellipse. The front part is characterized by an unstable zone of strong three-dimensional effects and intense mixing (Shringarpure et al., 2017). This fact is very important to the dynamics of the flow. The main causes of sediment mixing with the ambient fluid are gravitational and Kelvin-Helmholtz instabilities occurring at the head of the current (Britter and Simpson, 1978). Inside the head there is a divergence of flow caused by the movement of the fluid and the grains which dislocate the surrounding fluid. The body of the turbidity current travels with a velocity up to 40% higher than the velocity of the head. The tail, the third region of the current, is characterized by deceleration of the flow and dilution of the mixture (Manica, 2012; Simpson, 1997).

As turbidity currents propagate over the sea floor, they can trigger the evolution of a host of topographical features through deposition and erosion, such as channels, levees and sediment waves (Hall et al., 2008; Meiburg and Kneller, 2010). The generation of turbidity currents has

also been attributed to rivers in flood, when suspended sediment concentrations are high (Wright et al., 1986; Nash, 1994; Parsons et al., 2001, 2007; Mulder et al., 2003; Steel et al., 2016). The understanding of the behavior of non-conservative density currents is of utmost importance because they are largely responsible for the deposition of sediments in deep ocean waters, are directly involved in evolution of deep sea features, and are commercially important (e.g. as in petroleum reservoirs) (Kneller and Buckee, 2000; Alexander and Mulder, 2002).

One important aspect of the non-conservative density currents study is the comprehension of the role of different variables involved in the deposition processes and the structural characteristics of turbidity formation. Due to the difficulties of carrying out natural scale tests involving large and high-cost installations, small scale physical simulations in hydraulic tanks has often been used to extract valuable mechanistic information on turbidity current behavior (e.g. Simpson, 1997; Parker et al., 1987; Kneller and Buckee, 2000; Janocko et al., 2013).

The main objective of experimental simulations of non-conservative currents is to represent the resulting erosion, transport and deposition of sediment. The selection of the material to be deployed on the simulation of non-conservative currents must consider the size, density and settling velocity of the grains as principal criteria (Meiburg and Kneller, 2010).

Several materials have been used as sediment for the simulation of turbidity currents in small scales due to their similarity to natural sediment (Baas et al., 2016; Motanated and Tice, 2016; Janocko et al., 2013; Bursik and Woods, 2000; Rimoldi et al., 1996; Garcia and Parker, 1989; Middleton and Neal, 1989). These materials include: quartz powder (Altinakar et al., 1996; Janocko et al., 2013), silica (Garcia, 1994; Motanated and Tice, 2016) and glass (Garcia and Parker, 1989). These materials present effective behavior during the development of the turbidity current, with their density varying from 1500 to 2650 kg m^{-3}, settling velocity from 0.060 to 1.96 cm s^{-1} and diameter of the grains between 0.005 and 0.106 mm.

Coal is also commonly used in turbidity current simulations. Baas et al. (2016) reproduced the behavior of turbidity currents within a tank onto the horizontal bottom of a rectangular channel using coal particles. The coal particles had median grain sizes of 0.055 mm and a density of 1190 kg m^{-3}. Coal and water present similar specific masses, which increases the time for partial or complete deposition of the material in the tanks. However, coal has limitations due to its dark color, presenting a low contrast between sedimentary layers in the simulation tank. Despite the fact of coal being easily obtained commercially, other serious limitations are the control and reproducibility of parameters such as size and shape of the grains among different commercial lots (Baas et al., 2016; Manica, 2012). Synthesized materials are an alternative to natural products due to the possibility of controlling physical and hydraulic properties of the prepared materials and consequently improve the reproducibility in the simulations of turbidity currents. Hoyal and Sheets (2009) argued that the use of polymers may generate more realistic patterns of natural morphodynamic processes in small-scale experiments.

The behavior of the turbidity currents can also be simulated using polymeric and composite materials. Polymers are long chains of macromolecules, consisting of consecutive repeats of structural units known as mers (repeat unit). They are obtained by polymerization reactions in which molecules of monomers react with each other (Stroup-Gardiner and Newcomb, 1995). The composites consist of multiphase materials, whose constituent phases have chemical identity and different forms that remain distinct after processing. In addition, these phases are segregated by a defined interface. A polymeric composite consists of incorporating organic or inorganic fillers into a polymer matrix, resulting in a material with superior properties compared to the starting materials, such as improvement of thermal, mechanical and electrical properties. The polymer matrix confers the structure to the composite, while the filler acts by transferring its properties to the material

(Mohammad et al., 2009; Hussain et al., 2006).

Researchers have used some polymer materials in hydraulic simulations such as polymethyl methacrylate, which has a specific mass of 1180 kg m^{-3} and an average grain size of 0.6 mm (Kneller, 1995), as well as polyurethane with a specific mass of 1160 kg m^{-3}, an average grain size of 0.140 mm, and a settling velocity of 1.5 mm s^{-1} (Chamoun et al., 2017).

In the present work a composite was developed based on polyester resin to be used as artificial sediment in simulations of turbidity currents in hydraulic tanks, with a series of advantages over traditional natural materials, such as coal. Polyester resin obtained from styrene monomer was chosen due to its low cost, suitable mechanical properties and relatively low density combined with the possibility of coloring the polymeric matrix with different pigments in order to facilitate optical contrast between the deposited layers. In addition, a filler of high atomic number (barium sulphate, BaSO$_4$) was also added in order to obtain simultaneous contrast for x-ray imaging. Tuning of optical and x-ray contrast is possible through the variation of the dye color and barium concentration respectively.

2. Experimental methods

2.1. Materials

Barium chloride (Sigma-Aldrich), ethylene diamine tetraacetic acid (EDTA) (Sigma-Aldrich), chloridric acid (Merck) and sodium sulphate (Sigma-Aldrich) were used to create nanoparticles of barium sulphate. Orthophthalic unsaturated polyester resin (Arazyn; Fiberglass) and styrene monomer (Fiberglass), methylethyl ketone peroxide (Butanox M50; Fiberglass), and yellow and green pigments (Fiberglass) were used to produce the polymeric matrix.

2.2. Barium sulphate preparation

Nanoparticles of barium sulphate were prepared adapting methodologies described in Romero-Ibarra et al. (2010) and Bala et al. (2005). In a typical synthesis, 100 mL of 0.1 M barium chloride (BaCl$_2$) was mixed with 100 mL of 0.05 M EDTA under magnetic stirring at room temperature. The pH of the resulting solution was adjusted from 4.0 to 8.0 with hydrochloric acid (HCl). Thereafter, 100 mL of sodium sulphate (Na$_2$SO$_4$) was added to the mixture, which precipitated barium sulphate particles, and the resulting suspension was collected. The precipitated barium sulphate was separated from the mother liquor and washed with distilled water several times. The obtained particles were dried in an oven at 110 °C for 24 h for purification. This preparation resulted in a yield of 20% of barium sulphate (4.5 g).

2.3. Polyester resin nanocomposite preparation

The polyester resin composites with varying concentrations of barium sulphate were prepared by bulk polymerization. Bulk polymerization consists of adding a catalyst to the monomer without the addition of a solvent. The polymerization reaction occurs between a prepolymer containing unsaturated groups (orthophthalic unsaturated polyester resin) and styrene monomer which acts as a diluent for the prepolymer and catalyst (methyl ethyl ketone peroxide).

Before preparing the polyester resin, barium sulphate was dispersed in the styrene monomer to avoid the filler agglomeration. In order to transfer the filler properties to the polymer matrix it is necessary to achieve uniform dispersion and distribution. The filler (barium sulphate) was dispersed in the styrene monomer (2.5 g) in an ultrasonic device for 1 h. Then, the mixture was added to the orthophthalic unsaturated polyester resin (50 g) under mechanical stirring in order to obtain nanocomposites with different amounts of barium sulphate. Finally, the methyl ethyl ketone peroxide catalyst (1.5 g) was used to start the polymerization reaction in an ultrasonic device for 1 h. The

used barium sulphate concentrations were 0.5, 1.0, 2.0, 3.0, 4.0 and 5.0 wt% relative to the weight of orthophthalic unsaturated polyester resin.

The preparation of the composite with the pigments followed a similar procedure. The polyester resin was mixed with the monomer using a mechanical stirrer. Then, 0.5% (w/w) of the pigment was added to the mixture and the composite was submitted to an ultrasonic bath to disperse the dye and eliminate air bubbles that may occur. The catalyst was then added to the mixture to obtain the final composite.

2.4. Processing of the powders

After the polymerization, the nanocomposites were crushed and ground with two milling processes: first in a knife mill (model A1 basic, IKA) and then in a ball mill (model DL-MB, De Leo). The ground material was separated with a stainless steel mesh sieve set from 80 to 230 mesh, in order to obtain a particle diameter in a range of 0.177 to 0.063 mm, similar to the range used for coal.

2.5. Characterization techniques

The morphology of the composite powder and barium sulphate particles were analyzed by scanning electron microscopy (SEM) in a Philips XL30 equipment at 20 kV accelerating voltage in the secondary electron mode detection. The adapted picnometer methodology was used to measure the specific mass (Davidson and Perkin, 2013). The granular particles of the artificial sediments were characterized in triplicate at 20 °C, using ethanol (density 810 kg m^{-3}, 20 °C) as a displacement fluid. The x-ray data acquisitions tests were carried out in a microtomograph model Bruker Skyscan 1173, with micrometric resolution in the range of 6–7 mm, a peak voltage of 130 kV and a tungsten x-ray tube.

The settling velocities of the samples were determined based on the adapted methodology of Johnson et al. (1996) using a siltometer, also known as a settling column. Settling rate is measured with the siltometer as follows. First, the sample is placed within the vessel at the top of the equipment and released into the tube filled with tap water. The grains fall through the vertical column and reach the small basins at the rotatory tray underneath the column. After the grains reach the first basin, a gathering time interval is set. For these simulations, an interval of 30 s was used for each basin. The tray is then rotated so the grains fall into the second basin. The process was repeated until a full rotation of the tray was completed. Then, the deposited materials of all basins were collected in separate vessels, dried and individually weighed.

2.6. Hydraulic simulations

The hydraulic simulations were carried out in the small tanks at the facilities of the Hydraulic Research Institute at the Federal University of Rio Grande do Sul, Brazil. Turbidity currents were simulated using a rectangular channel, with dimensions of 0.3 m long, 0.125 m wide and 0.15 m height (Fig. 1). A feeding tank (in the form of a funnel) was used and the simulating material into the tank. The first run was made with the yellow composite, producing a layer with roughly 0.6 mm at the bottom of the tank. After sedimentation, a turbidity current containing
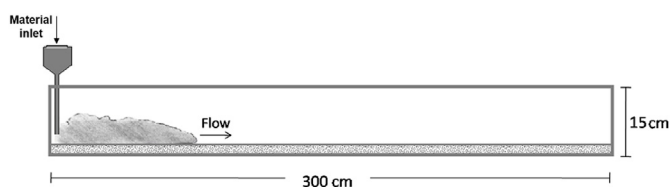

Fig. 1. Schematic diagram of the tank used to simulate turbidity currents (adapted of Baas et al., 2005).

green particles was released in order to obtain a second sediment layer. The sediment concentration in the currents was 3 vol%. Video cameras recorded the flow-bed interactions and depositional processes. The acquisition of the optical images was performed with DCR-TRV cameras (models 110 and 120).

3. Results and discussion

3.1. Barium sulphate/polyester resin nanocomposites

Fig. 2 shows SEM images of the synthesized barium sulphate particles deposited on carbon substrates after dispersion by sonification. Each particle appears to be formed by the agglomeration of smaller grains with average size approximately 80 nm (Fig. 2b).

Different amounts of barium sulphate particles were dispersed in the polyester resin during mass polymerization, resulting in composites containing 0.5%, 1.0%, 2.0%, 3.0%, 4.0% and 5.0% (w/w) of the $BaSO_4$ relative to the resin mass. The final product is a block of solid material, as shown in Fig. 3. After grinding, the composite powder presented, according to the classification proposed by Tucker (2001), either semi-rounded or semi-angular morphology (Fig. 2b).

The preparation of the materials described in this work is relatively simple and of low cost (\$ 5.00/kg of polyester resin). The materials commonly used in studies of turbidity currents, such as coal and crushed silica, are materials of natural origin, they are abundant and cost less than the composite prepared in this work. However, such naturally occurring materials cannot be modified as the polymeric materials. The polyester resin prepared in this work has a simple preparation method and presents a low-cost similar already used in studies of turbidity currents (polymethyl methacrylate and polyurethane). The differential of this work is the incorporation of filler or pigment in the polymeric matrix in order to improve the optical contrast between the deposited layers.

3.2. Specific mass and settling velocity of barium sulphate/polyester resin nanocomposites

The specific mass and settling velocity of the composite powders are essential parameters to determine the hydraulic and depositional behavior of the generated flows and simulated sedimentary deposits (Table 1). The specific mass of the composite resins have an average value of 1096 kg m^{-3} for samples of polyester resin with barium sulphate, 1100 kg m^{-3} for samples of pure polyester resin and 1030 kg m^{-3} for samples of polyester resin with pigmentation. This range of values is within levels of specific mass considered satisfactory for simulations in hydraulic tanks as the results meet the specific mass values of the materials currently used in this sort of simulation.

Concerning the settling velocity (Table 1), the mean value obtained for powders with a particle size range as from 0.063 to 0.177 mm was 0.0109 m s^{-1} for the polyester resin with 5.0% barium sulphate, and 0.011 m s^{-1} for the resin pigmented with the dyes. Although the settling velocity obtained was slightly higher than that reported for coal (0.010 m s^{-1}) (Manica et al., 2012), there is a hydrodynamic equivalence between the materials, as the results differ by only ~10%.

The morphological and hydraulic characterization of the composites demonstrates that the material meets the necessary properties to be used in simulations of turbidity currents. The combined results indicate that the prepared composites are suitable as a replacement for traditional materials for it is possible to employ dimensional scaling to compare the properties of the fluid flows.

3.3. Hydraulic simulations and imaging contrast

The hydraulic tests were conducted using the pigmented composites prepared with yellow and green dye. The synthesized materials formed turbidity currents after being released from the head of the simulation
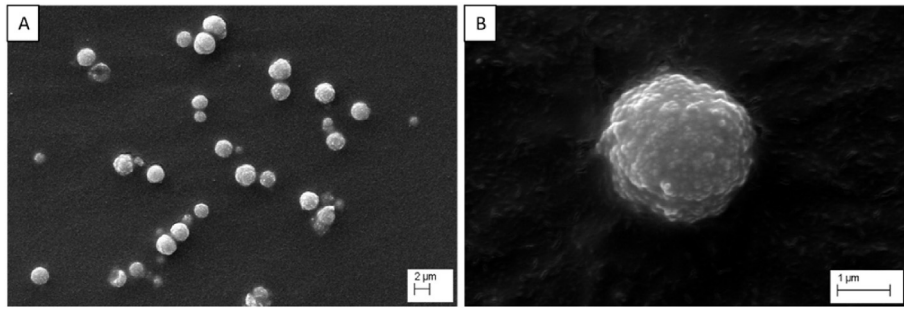
Fig. 2. SEM images of barium sulphate particles with magnification (a) 5000x; (b) 35000x.

Fig. 3. Block of solid materials before the breaking and milling process.

Table 1
Characteristics of prepared materials.

Samples	Percentage of $BaSO_4$ (%)	Density (kg.m^{-3})	Settling velocity (cm.s^{-1})
Polyester resin/$BaSO_4$	0.5	1120	0.0109
Polyester resin/$BaSO_4$	1.0	1090	–
Polyester resin/$BaSO_4$	2.0	1080	–
Polyester resin/$BaSO_4$	3.0	1160	–
Polyester resin/$BaSO_4$	4.0	1100	–
Polyester resin/$BaSO_4$	5.0	1090	–
Pure polyester resin	0	1100	0.0012
Polyester resin/ pigments	0	1030	0.0011

tank, as previously described (Fig. 4a). Subsequent to deposition of the yellow grains, a turbidity current containing the green pigment was released (Fig. 4b). Newtonian fluxes were formed with a series of vortices along the currents direction of flow. Such fluxes are formed from the viscous shear at the upper interface of the current with the ambient fluid, creating a zone of turbulent mixing behind the head of the turbidity current (Middleton, 1993). Fig. 4a shows a well-defined head with intense vortices behind it, indicating a zone of high mixing. Due to the high turbulence intensity, the sediment is kept in suspension. This type of head occurs because of the high resistance of the ambient fluid under the flow and the gravitational forces acting on the body of the turbidity current. At the final stage of the flow, the velocity of the turbidity current decreases causing deposition of sediment (Kneller and Buckee, 2000; Manica, 2012; Nogueira et al., 2014; Zavala and Arcuri, 2016). In the second run, when green sediments moved on top of the older yellow sediments (Fig. 4b), a decrease in head height compared to the first launch was observed (Fig. 4a). This decrease is caused by the increased speed and buoyancy flux, resulting in equivalent average velocities for the head and turbidity current body. This type of turbidity current profile is characterized by the formation of an inner grain layer
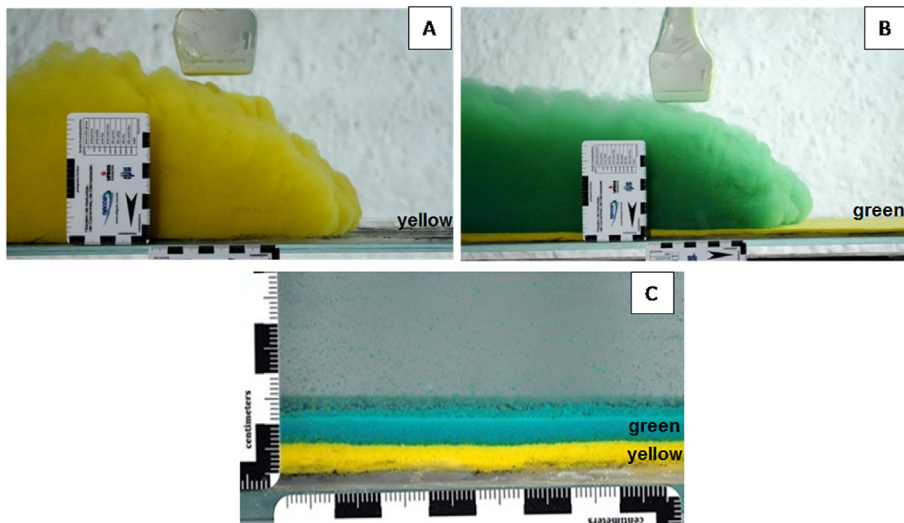

Fig. 4. Simulation result of the turbidity currents with the polyester composites with (a) yellow pigments and (b) green. (c) Final configuration of deposits in the hydraulic simulation tank with the green sediments on the top layer and the yellow on the bottom layer. (For interpretation of the references to color in this figure legend, the reader is referred to the Web version of this article.)
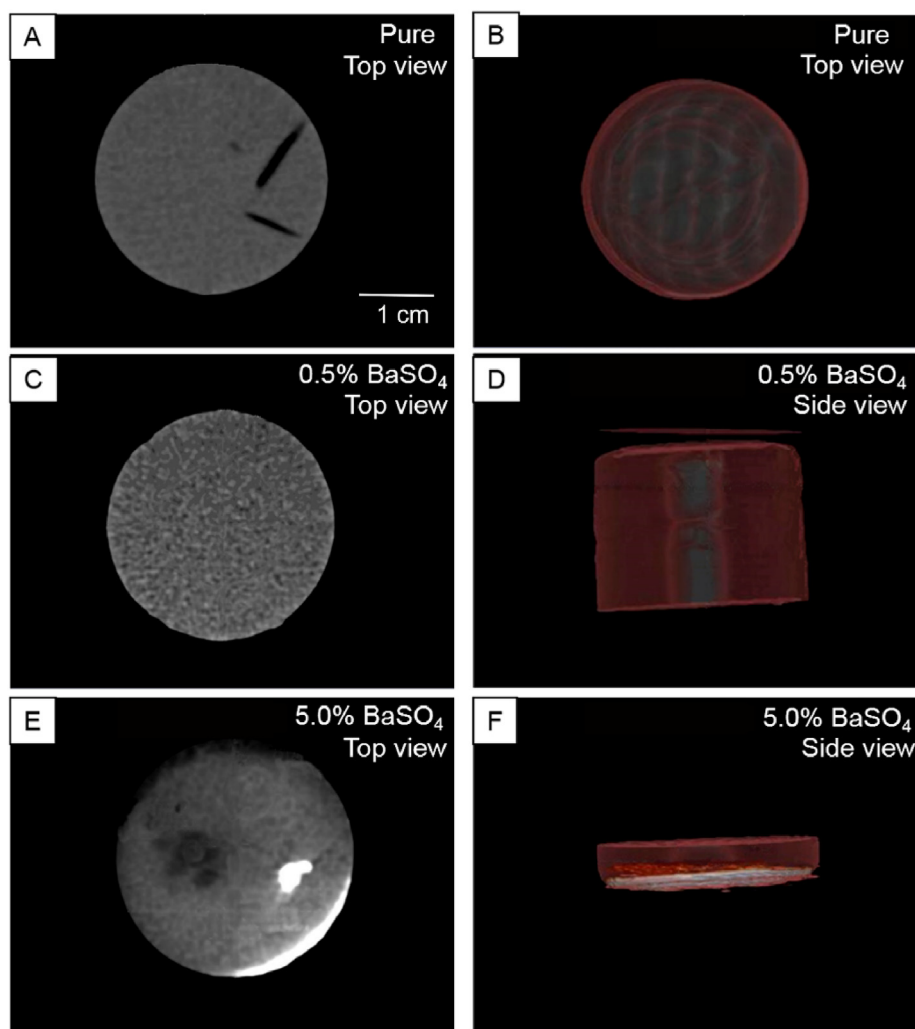
Fig. 5. Images of x-ray tomography: (a) pure polyester resin – top view; (b) pure polyester resin – top view; (c) 0.5% BaSO₄ polyester resin – top view; (d) 0.5% BaSO₄ polyester resin – side view; (e) polyester resin with 5.0% BaSO₄ – top view; (f) 5.0% BaSO₄ polyester resin – side view. The scale bar in (a) applies to all images.

concentrated near the bottom. The magnitudes of forces acting on the head (buoyancy) and over the body (gravitational) are similar, reducing the height of the head of the current. The flow generates a strong and concentrated undulating layer near the bottom, creating a bipartite flow that deposited a large amounts of the sediments suddenly (high deposition rate) (Zavala and Arcuri, 2016; Manica, 2012).

The current simulated with the synthetic materials can be classified as non-cohesive Newtonian flux. This characteristic plus the low concentration of particles affects the flow dynamics and deposition. Simulations employing non-cohesive fine grained sand behaved in a similar way (Manica, 2012). Such essays were carefully studied using velocity detectors spreaded out over the tank. They indicated an increase in velocity and buoyancy flow values. The nearness of the body and head velocities indicates that the buoyancy forces on the head are balanced by the gravitational forces. An intense mixing zone happens in the flow head. After the high velocity values are reached, a strong deceleration takes place, stopping the flow. This strong deceleration must be a result from the formation of a layer of grains within the flow head. Such beds tend to concentrate at the bottom due to friction with the previously deposited bed, which in turn depletes the kinetic energy of the flow. The velocity difference between the bottom layer and the rest of the flow implies different mechanisms of deposition.

The grain support mechanisms in the turbidity currents represented by the photographs in Fig. 4 are classified as turbulent flow (generated in the head) and Kelvin-Helmholtz instabilities (behind the head and

along the layer of mixtures on the upper and lower surfaces) (Kneller and Buckee, 2000; Mazumder, 2003; Baas et al., 2005, 2011). These grain support mechanisms are not valid for the final stages of the flow, in which the current decelerates (Manica, 2012; Baas et al., 2016; Zavala and Arcuri, 2016).

The final configuration of the simulation is shown in Fig. 4c. The green material deposits smoothly on top of the flat yellow layer. In addition, a thin sediment layer of the green composite of approximately 1.0 mm in height was formed too. This layer is formed by the sediments that remained floating in the tank due the in smaller size. Through the images, it is possible to easily observe the contrast between the colored layers of the sediments. The height of the yellow lamina was around 6.0 mm and the lamina with the green pigment, around 5.0 mm. Successive deposits can be performed with polymers containing dyes of various colors, allowing clear optical contrast for photography and the visual inspection without the use of supplementary equipment. Such features would not only speed evaluation of the final deposit architecture, but also permit additional analysis, such as intermixing between different deposition laminas.

In addition to the optical contrast, preliminary studies were performed that demonstrate the contrast in properties of the composite resins during x-ray imaging (Fig. 5). Due to its large penetration and very small wavelength, x-ray imaging may add high-resolution spatial information of the deposits, even across large volume tanks, provided the x-ray photons have large enough energy. X-ray contrast is also
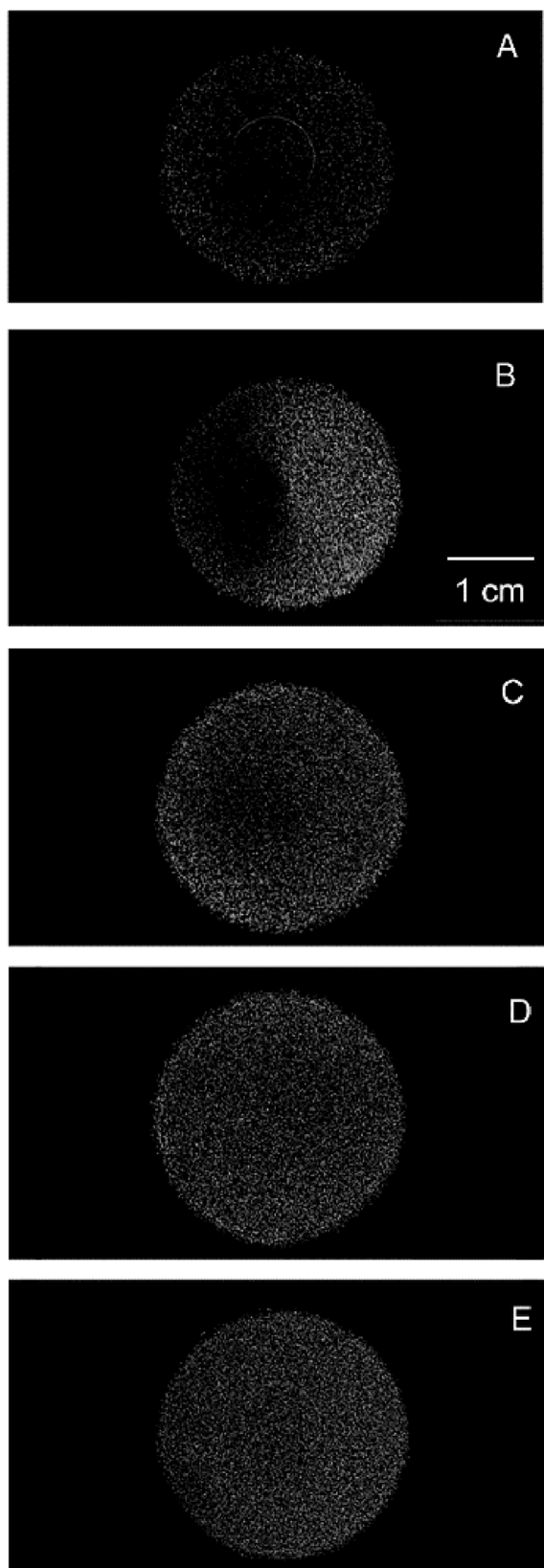
Fig. 6. X-ray microtomography images of the polyester resin with (a) 1.0%, (b) 2.0%, (c) 3.0%, (d) 4.0% and (e) 5.0% of barium sulphate (w/w). Granulometric range of grains: 150–250 μm. The scale bar in (b) applies to all images.

useful because of the tomographic technique capabilities, which allows collection of 3D information and post processing slicing in arbitrary planes.

X-ray tomography allowed the imaging of the barium sulphate filler added to the polyester resin. The X-ray tomography presented images (Fig. 5) refer to pure polyester resin, 0.5% barium sulphate polyester resin and resin polyester with 5.0% (w/w) barium sulphate. Fig. 5a and b were obtained for the polyester resin without filler addition. One should notice that no contrast is displayed. Fig. 5c and d show little contrast, observed in small white spots on the images, referring to the addition of 0.5% (m/m) of the barium sulphate filler. Already in Fig. 5e and f, it is possible to visualize strong opacity, represented by the white parts in the images. In Fig. 5e, the presence of barium sulphate is very clear and concentration of the particles on one side of the block is observed. In Fig. 5f, it can be seen that the filler was concentrated at the bottom of the block. This occurred because the dispersion of the filler in the polymer matrix was not homogeneous.

The contrast's results of the pure composite powders were obtained through an x-ray microtomography equipment. The technique was used to study the contrast of the ground nanocomposites. Microtomographies of the resins with different concentrations of barium sulphate are presented in Fig. 6. For the composite with 0.5% of the filler, there is almost no contrast between the polymeric matrix and the filler (not shown in Fig. 6). As expected, the increase in the concentration of barium sulphate provides an increase in the opacity of the sample to the x-rays (greater attenuation depicted as white) which appears more uniformly throughout the samples. For the x-ray accelerating voltage used here (130 kV), addition of 2% of particles of barium sulphate in the polymeric matrix already provides the necessary attenuation for a good contrast to the pure polymeric resin. The amount of filler for obtaining optimal contrast will, of course, depend on the size of the simulation tank and x-ray acceleration voltage used and is a matter of future investigation.

Our preliminary results demonstrate the great potential of the produced composite polymer to be used as synthetic sediments. Such multifunctional materials provide enhanced capabilities for imaging of the deposits with non-invasive and non-destructive techniques, which can be applied separately or simultaneously. The versatility of the polymer composite can be easily tuned for optical or x-ray contrast with the use of various dyes and different amounts of the filler, respectively. Therefore, a variety of the material with similar hydraulic and morphological properties, but distinct contrast properties can be prepared and used in physical simulations facilitating not only the investigation of the final deposit architecture, but also possible dynamic features that occur in between layers during deposition.

4. Conclusions

The characterization tests for the pure polyester resin, polyester resin with inorganic filler and polyester resin with pigmentation prove that the materials can be used in substitution of the coal in simulations of turbidity currents because they generated turbidity currents with a similar hydraulic behavior to coal. The nanocomposite prepared with resin and barium sulphate presented small variations in the hydraulic characteristics in comparison to the neat resin tests. For this reason, the material can be used for future hydraulic simulations using non-invasive methodologies, allowing high contrast between layers containing barium sulphate and the pure material. The incorporation of nanometric scale filler and dye to the matrix did not present significant changes in the parameters of specific mass and settling velocity, important characteristics that allow the material to be used in substitution of coal. The x-ray microtomographies tests showed that the objective of producing a polymeric nanocomposite with inorganic filler for use in non-destructive tests was reached. The composites of polyester resin and barium sulphate presented contrast in x-ray tomography images. This result shows that for this application and in this polymer matrix,

the composites are an innovative material due to its potential use in the study of non-conservative turbidity currents.

Acknowledgment

Appendix A. Supplementary data

Supplementary data to this article can be found online at https://doi.org/10.1016/j.marpetgeo.2019.104140.

References

Alexander, J., Mulder, T., 2002. Experimental quasi-steady density currents. Mar. Geol. 186, 195–210.

Allen, J.R.L., 1971. Mixing at turbidity current heads, and its geological implications. J. Sediment. Petrol. 41, 97–113.

Altinakar, M.S., Graf, W.H., Hopfinger, E.J., 1996. Flow Structure in turbidity currents. J. Hydraul. Res. 34, 713–718.

Baas, J.H., Manica, R., Puhl, E., Borges, A.L.O., 2016. Thresholds of intrabed flow and other interactions of turbidity currents with soft muddy substrates. Sedimentology 63, 2002–2036.

Baas, J.H., et al., 2005. Coupling between suspended sediment distribution and turbulence structure in a laboratory turbidity current. J. Geophys. Res. 110, C11015.

Baas, J.H., et al., 2011. Depositional processes, bedform development and hybrid bed formation in rapidly decelerated cohesive (mud-sand) sediment flows. Sedimentology 58, 1953–1987.

Bala, H., Fu, W., Zhao, J., Ding, X., Jiang, Y., 2005. Preparation of BaSO$_4$ nanoparticles with self-dispersing properties. Colloid. Surf. Physicochem. Eng. Asp. 252, 129–134.

Britter, R.E., Simpson, J.E., 1978. Experiments on the dynamics of a gravity current head. J. Fluid Mech. 88, 223–240.

Bursik, M.I., Woods, A.W., 2000. The effects of topography on sedimentation from particle-laden turbulent density currents. J. Sediment. Res. 70 (1), 53–63.

Chamoun, S., De Cesare, G., Shleiss, A.J., 2016. Managing reservoir sedimentation by venting turbidity currents: a review. Int. J. Sediment Res. 31, 195–204.

Chamoun, S., De Cesare, G., Schleiss, A.J., 2017. Management of turbidity current venting in reservoirs under different bed slopes. J. Environ. Manag. 204, 519–530.

Davidson, S., Perkin, M., 2013. An investigation of density determination methods for porous materials, small samples and particulates. Measurement 46, 1766–1770.

Garcia, M., Parker, G., 1989. Experiments on hydraulic jumps in turbidity currents near a canyon-fan transition. Science 245 (C3), 393–396.

Garcia, M.H., 1994. Depositional turbidity currents laden with poorly sorted sediment. J. Hidraul. Eng. 120 (11), 1240–1263.

Hall, B., Meiburg, E., Kneller, B., 2008. Channel formation by turbidity currents: Navier-Stokes-based linear stability analysis. J. Fluid Mech. 615, 185–210.

Hansen, L.A.S., Callow, R.H.T., Kane, I.A., Gamberi, F., Rovere, M., Cronin, B.T., Kneller, B.C., 2015. Genesis and character of thin-bedded turbidites associated with submarine channels. Mar. Pet. Geol. 67, 852–879.

Hoyal, D.C.J.D., Sheets, B.A., 2009. Morphodynamic evolution of experimental cohesive deltas. J. Geophys. Res. 114 (F2), 1–18.

Hussain, F., Hojjati, M., Okamoto, M., Gorga, R.E., 2006. Polymer-matrix nanocomposites, processing, manufacting and application: an overview. J. Compos. Mater. 40, 1511–1575.

Janocko, M., Cartigny, M.B.J., Nemec, W., Hansen, E.W.M., 2013. Turbidity current hydraulics and sediment deposition in erodible sinuous channels: laboratory experiments and numerical simulations. Mar. Pet. Geol. 41, 222–249.

Johnson, C.P., Li, X., Logan, B.E., 1996. Settling velocities of fractal aggregates. Environ. Sci. Technol. 30 (6), 1911–1918.

Kneller, B., 1995. Beyond the turbidite paradigm: physical models for deposition of turbidites and their implications for reservoir prediction. Geol. Soc. Spec. Publ. 94, 31–49.

Kneller, B., Buckee, C., 2000. The structure and fluid mechanics of turbidity currents: a review of some recent studies and their geological implications. Sedimentology 47 (1), 62–94.

Manica, R., 2012. ISBN: 978-953-307-893-9 In: Schulz, Harry (Ed.), Sediment Gravity Flows: Study Based on Experimental Simulations, Hydrodynamics -Natural Water Bodies. InTech Available from: http://www.intechopen.com/books/hydrodynamics-natural-water-bodies/sediment-gravity-flows-study-basedon-experimental-simulations.

Mazumder, R., 2003. Sediment transport, aqueous bedform stability and morphodynamics under unidirectional current: a brief overview. J. Afr. Earth Sci. 36, 1–14.

Meiburg, E., Kneller, B., 2010. Turbidity currents and their deposits. Annu. Rev. Fluid Mech. 42, 135–156.

Middleton, G.V., 1993. Sediment deposition from turbidity currents. Annu. Rev. Earth Planet Sci. 21, 89–114.

Middleton, G.V., Neal, W.J., 1989. Experiments on the thickness of beds deposited by turbidity currents. J. Sediment. Petrol. 59, 297–307.

Mohammad, H.B., Vafayan, M., Poorabdollah, M., 2009. Low profile unsatured polyester resin-clay nanocomposite properties. Polym. Compos. 30, 629–638.

Motanated, K., Tice, M.M., 2016. Hydraulic evolution of high-density turbidity currents from the Brushy Canyon Formation, Eddy County, New Mexico inferred by comparison to settling and sorting experiments. Sediment. Geol. 337, 69–80.

Mulder, T., Syvitski, J.P.M., Migeon, S., Faugères, J.C., Savoye, B., 2003. Marine hyperpycnal flows: initiation, behavior and related deposits. A review. Mar. Pet. Geol. 20, 861–882.

Nash, D.B., 1994. Effective sediment-transporting discharge from magnitude-frequency analysis. J. Geol. 102, 79–95.

Nogueira, H.I.S., Adduce, C., Alves, E., Franca, M.J., 2014. Dynamics of the head of gravity currents. Environ. Fluid Mech. 14 (2), 519–540.

Parker, G., Garcia, M., Fukushima, Y., Yu, W., et al., 1987. Experiments on turbidity currents over an erodible bed. J. Hydraul. Res. 25 (1), 123–147. https://doi.org/10.1080/00221688709499292.

Parsons, J.D., Bush, J.W.M., Syvitski, J., 2001. Hyperpycnal plume formation from riverine outflows with small sediment concentrations. Sedimentology 48, 465–478.

Parsons, J.D., Friedrichs, C.T., Traykovski, P.A., Mohrig, D., Imran, J., Syvitski, J.P.M., Parker, G., Puig, P., Buttles, J.L., García, M.H., 2007. The mechanics of marine sediment gravity flows. In: Nittrouer, C.A., Austin, J.A., Field, M.E., Kravitz, J.H., Syvitski, J.P.M., Wiberg, P.L. (Eds.), Continental Margin Sedimentation: from Sediment Transport to Sequence Stratigraphy. Blackwell Publishing Ltd., Oxford, UK.

Rimoldi, B., Alexander, J., Morris, S., 1996. Experimental turbidity currents entering density-stratified water: analogues for turbidites in Mediterranean hiper saline basins. Sedimentology 43, 527–540.

Romero-Ibarra, I.C., Rodriguez-Gattorno, G., García-Sanchez, M.F., Sánchez-Solís, A., Manero, O., 2010. Hierarchically nanostructured barium sulfate fibers. Langmuir 26, 6954–6959.

Shringarpure, M., Cantero, M.I., Balachandar, S., 2017. Equivalence of turbulence statistics between monodisperse and polydisperse turbidity currents. Adv. Water Resour. 3, 1–15.

Simpson, E.J., 1997. Gravity Currents in the Environment and the Laboratory, 2 ed. Cambridge University, pp. 244p.

Simpson, J.E., Britter, R.E., 1979. The dynamics of the head of a gravity current advancing over a horizontal surface. J. Fluid Mech. 94, 477–495.

Steel, E., Simms, A.R., Warrick, J., Yokoyama, Y., 2016. Highstand shelf fans: the role of buoyancy revers al in the deposition of a new type of shelf sand body. GSA Bull. 128, 1717–1727.

Stroup-Gardiner, M., Newcomb, D.E., 1995. Polymer Literature Review. University of Minnesota, Minnesota.

Tucker, M.E., 2001. Sedimentary Petrology: an Introduction to the Origin of Sedimentary Rocks, third ed. Wiley-Blackwell, pp. 272.

Wright, L.D., Yang, Z.S., Bornhold, B.D., Keller, G.H., Prior, D.B., Wiseman, W.J., 1986. Hyperpycnal plumes and plume fronts over the huanghe delta front. Geo Mar. Lett. 6, 97–105.

Zavala, C., Arcuri, M., 2016. Intrabasinal and extrabasinal turbidites: origin and distinctive characteristics. Sediment. Geol. 337, 36–54.